Development of Silica/Vanadia/Titania Catalysts for Removal of Elemental Mercury from Coal-Combustion Flue Gas

YING LI,[†] PATRICK D. MURPHY,[‡] CHANG-YU WU,*[,†] KEVIN W. POWERS,[§] AND JEAN-CLAUDE J. BONZONGO[†]

Department of Environmental Engineering Sciences, University of Florida, Department of Chemical Engineering, University of Florida, and Particle Engineering Research Center, University of Florida

Received January 11, 2008. Revised manuscript received March 26, 2008. Accepted May 5, 2008.

$SiO_2/V_2O_5/TiO_2$ catalysts were synthesized for removing elemental mercury (Hg^0) from simulated coal-combustion flue gas. Experiments were carried out in fixed-bed reactors using both pellet and powder catalysts. In contrast to the SiO_2-TiO_2 composites developed in previous studies, the V_2O_5 based catalysts do not need ultraviolet light activation and have higher Hg^0 oxidation efficiencies. For Hg^0 removal by $SiO_2-V_2O_5$ catalysts, the optimal V_2O_5 loading was found between 5 and 8%, which may correspond to a maximum coverage of polymeric vanadates on the catalyst surface. Hg^0 oxidation follows an Eley–Rideal mechanism where HCl, NO, and NO_2 are first adsorbed on the V_2O_5 active sites and then react with gas-phase Hg^0. HCl, NO, and NO_2 promote Hg oxidation, while SO_2 has an insignificant effect and water vapor inhibits Hg^0 oxidation. The $SiO_2-TiO_2-V_2O_5$ catalysts exhibit greater Hg^0 oxidation efficiencies than $SiO_2-V_2O_5$, may be because the V–O–Ti bonds are more active than the V–O–Si bonds. This superior oxidation capability is advantageous to power plants equipped with wet-scrubbers where oxidized Hg can be easily captured. The findings in this work revealed the importance of optimizing the composition and microstructures of SCR (selective catalytic reduction) catalysts for Hg^0 oxidation in coal-combustion flue gas.

Introduction

Coal-fired utility boilers are currently the largest single-known source of anthropogenic mercury (Hg) emissions in the United States, accounting for one-third of the 150 tons of Hg emitted annually (*1*). In 2005 the U.S. EPA issued the Clean Air Mercury Rule (CAMR) to cap and reduce Hg emissions from coal-fired power plants; meanwhile, it reversed its December 2000 finding that it was "appropriate and necessary" to regulate coal- and oil-fired power plants for Hg emissions (*2*). In February 2008, the U.S. Court of Appeals for the District of Columbia vacated both the reversal and the CAMR (*3*). While it takes time for the U.S. EPA to establish new rules, a significant number of U.S. states have enacted their own Hg emissions regulations, which are generally more stringent than the CAMR.

In the coal-derived flue gas, there are three basic forms of Hg: elemental Hg (Hg^0), oxidized Hg (Hg^{2+}) and particle-bound Hg (Hg_p) (*4*). Hg_p can be collected in electrostatic precipitators (ESPs) and/or baghouses. Hg^{2+} is soluble in water and is readily captured by wet flue gas desulfurization (FGD) equipment. Hg^0 is volatile and insoluble in water, and thus, it is poorly captured using conventional control technologies. Unfortunately, Hg speciation studies showed that Hg^0 is the dominant species in flue gas when burning low rank (subbituminous or lignite) coals. Therefore, need exists for a low cost Hg oxidation/capturing process.

Activated carbon injection (ACI) is one of the major commercially available technologies for Hg control from coal-fired power plants. However, the incremental cost of Hg control via ACI is estimated to range from $3810 to $166 000/lb Hg removed (*5*). A variety of noncarbon based Hg^0 oxidation catalysts have also been studied, which fall into two groups: SCR catalysts (typically composed of V_2O_5/WO_3 supported on TiO_2), and metals and metal oxides (*6*). SCR catalysts were found to oxidize Hg^0 at their typical operating temperatures (300∼400 °C), particularly in the presence of HCl (*7–10*). Lee et al. (*8*) reported that Hg^0 oxidation across a pilot-scale SCR facility reached ∼90% burning three Illinois bituminous coals (HCl > 100 ppm in flue gas) but was less than 20% burning a Powder River Basin (PRB) subbituminous coal (HCl = 7.9 ppm). Blythe et al. (*11*) demonstrated that SCR catalysts can also oxidize Hg^0 at low temperatures (∼130 °C) upstream of pilot-scale wet FGD systems; however, their activities (∼67% Hg^0 oxidation for fresh catalysts) were lower than those of palladium and certain carbon-based catalysts (>95% Hg^0 oxidation) when burning North Dakota lignite. Although the mechanisms of Hg^0 oxidation over SCR catalysts are not clear to date, V_2O_5 species supported on TiO_2 is believed to be the active phase of SCR catalysts for the reduction of NO by NH_3 (*12–14*). The amount of V_2O_5 in commercial SCR catalysts is generally less than 1 wt% (*14*), but it was reported that 8 wt% V_2O_5 loading corresponded to the highest SCR activity for NO reduction at low temperatures (<250 °C) (*15*). Similarly, V_2O_5 loading may play a significant role in low temperature SCR activity for Hg oxidation. On the other hand, the nature of the support for V_2O_5 is also an important factor for SCR catalytic activity (*13*). TiO_2 as a support normally has drawbacks such as low surface area; hence, a common practice is to use a SiO_2 support coated with TiO_2 (*16*).

As a novel metal oxide catalyst for Hg^0 oxidation, TiO_2-based nanomaterials (in situ generated TiO_2 nanoparticles and SiO_2-TiO_2 nanocomposites) under UV irradiation have demonstrated greater than 90% Hg^0 removal under room conditions (*17, 18*). Follow-up studies by Li et al. (*19–21*) indicated that flue gas components significantly affect Hg capture on SiO_2-TiO_2 composites (12 wt% TiO_2), with HCl and SO_2 enhancing Hg^0 oxidation while water vapor and NO_x having inhibitory effects. The detrimental effect of NO that only 50 ppm NO reduced Hg^0 oxidation to 10% (using 8 g SiO_2-TiO_2) necessitates adding more active species to the composite (*19*).

Since both commercial SCR catalysts and the SiO_2-TiO_2 composites have their limitations on Hg^0 oxidation in coal-combustion flue gas, this study aimed to enhance the catalytic activity by incorporating V_2O_5 into the SiO_2-TiO_2 composites. The synthesized $SiO_2/V_2O_5/TiO_2$ catalysts take the advantage of high surface area SiO_2 support over the SCR catalysts. The optimal V_2O_5 loading of the synthesized catalysts was

* Corresponding author phone: 352-392-0845; fax: 352-392-3076; e-mail: cywu@ufl.edu.
[†] Department of Environmental Engineering Sciences.
[‡] Department of Chemical Engineering.
[§] Particle Engineering Research Center.

10.1021/es8000272 CCC: $40.75
Published on Web 06/11/2008

explored. The effects of individual flue gas components on the catalytic performance were investigated as well. While commercial SCR catalysts are usually tested "as received" with little information reported on their chemical composition and microstructures, findings in this study would contribute to fabrication of more effective SCR catalysts for Hg^0 oxidation through optimization of catalyst properties.

Materials and Methods

Catalyst Preparation. The procedure of synthesizing the SiO_2-TiO_2 composite using a sol−gel method was reported in detail in our previous studies (*20*). When synthesizing the $SiO_2-TiO_2-V_2O_5$ composite, vanadium triisopropoxide oxide (VTPO) (Alfa Aesar) was added as the precursor of V_2O_5. A known amount of VTPO was first dissolved in well stirred ethanol to form an orange-brown solution. It was then added dropwise to the prepared silica sol under vigorous stirring. TiO_2 nanoparticles (P25, Degussa) were finally added to the mixture before it started to gel. When synthesizing the $SiO_2-V_2O_5$ composite, the step of adding TiO_2 nanoparticles was skipped. The composites were originally made in the pellet form (3 mm in diameter and 5 mm in length). A powder form of the composites was also obtained by grinding the pellets and sieving through 40/100 meshes (425/150 μm). The catalysts are abbreviated by way of ST*x*V*y*, where S represents SiO_2, T represents TiO_2, V represents V_2O_5, and *x* and *y* represent the weight percentages of the TiO_2 and V_2O_5, respectively.

Powder Characterization. The BET surface areas of the powder catalysts were measured using a Quantachrome NOVA1200 gas sorption analyzer (Boynton Beach, FL). It is assumed that the pellets and powder have equivalent specific surface areas due to their highly porous structure. X-ray diffraction (XRD) patterns of the powders were recorded with a Philips APD 3720 diffractometer using Cu Kα radiation (λ = 0.1542 nm) in the range of 15−40° (2θ) with a step size of 0.02°. X-ray photoelectron spectroscopy (XPS) analysis of the samples was carried out by a Perkin-Elmer PHI 5100 ESCA system using Mg Kα ($h\nu$ = 1253.6 eV) radiation to excite photoelectrons.

Catalyst Activity Measurement. As reported in our previous studies (*19*–*22*), the SiO_2-TiO_2 composite needs activation by UV light. Thus, the dependence of UV light activation for V_2O_5 based composites was first investigated. Pellet form of the catalysts was used because the space between the pellets allows better penetration of UV light to achieve maximum exposure of the catalyst to the light. However, if tests indicate that the UV light is unnecessary, the powder form is preferable because of better contact of the gas with the material's inner pore surfaces.

Table 1 summarizes the experimental conditions, and Figure 1 shows the experimental system. In set I, the three catalysts in pellet form were tested using a UV reactor. Two simulated flue gases, FG1 and FG2, were introduced, with composition in the range of those burning high and low rank coals, respectively. All the flue gas components were supplied by certified gas cylinders, and their flow rates were controlled by mass flow controllers (MFCs). The source of Hg^0 vapor was a Dynacal Hg^0 permeation device (VICI Metronics) immersed in a constant-temperature (90 ± 0.2 °C) water bath. Water vapor was introduced from a heated water bubbler. The UV reactor consists of a UV lamp and a U-shape quartz reactor where the pellet catalysts were packed. A RA-915+ Hg analyzer (OhioLumex) coupled with a Hg speciation conversion system were used to measure gas-phase Hg speciation downstream the reactor. Details of the experimental setup for testing pellet catalysts were reported in our previous study (*19*).

In set II, catalysts in powder form were tested with a modified reactor (without UV light) as shown in the inset of Figure 1. The U-tube quartz reactor was immersed in an oil bath heated by a hotplate to a constant temperature of 135 °C (±0.5 °C). The catalyst powders were packed in between glass wools in the reactor. FG3 was used as the simulated flue gas which is also in the range of those burning low rank coals but has a lower water vapor concentration than FG2.

Finally, to explore the reaction mechanisms and the roles of the flue gas components in the catalytic reactions, the catalytic activity of a fixed amount of catalyst (SV5) was examined with introduction of individual flue gas components (set III).

TABLE 1. Experimental Conditions for Activity Measurement of the Catalysts

	catalyst	form	reactor	mass (g)	carrier gas[a]
set I	ST12	pellet	UV	8.0	FG1[b], FG2[c]
	SV2	pellet	UV	8.0	FG1, FG2
	ST12V2	pellet	UV	8.0	FG1, FG2
set II	SV2	powder	non-UV	0.50	FG3[d]
	SV5	powder	non-UV	0.50	FG3
	SV8	powder	non-UV	0.50	FG3
	SV10	powder	non-UV	0.50	FG3
	ST12V5	powder	non-UV	0.50	FG3
	ST12V2	powder	non-UV	0.50	FG3
	ST6V5	powder	non-UV	0.50	FG3
	ST18V5	powder	non-UV	0.50	FG3
set III	SV5	powder	non-UV	0.25	individual gas (O_2, HCl, NO, NO_2, SO_2, or H_2O) at varied conc.

[a] Containing 15∼16.5 ppb Hg^0 balanced with N_2 in all tests; total flow rate = 1.5 lpm. [b] FG1 = 4% O_2, 12% CO_2, 8% H_2O, 30 ppm HCl, 1200 ppm SO_2, 300 ppm NO, 10 ppm NO_2. [c] FG2 = 4% O_2, 12% CO_2, 12% H_2O, 10 ppm HCl, 400 ppm SO_2, 300 ppm NO, 10 ppm NO_2. [d] FG3 = 4% O_2, 12% CO_2, 8% H_2O, 10 ppm HCl, 400 ppm SO_2, 300 ppm NO, 10 ppm NO_2.

It is generally agreed that the decrease in Hg^0 concentration across the catalysts is due to Hg^0 oxidation, and thus, the oxidation efficiency (E_{oxi}) is defined as (*7*, *9*)

$$E_{oxi}(\%) = \frac{\Delta Hg^0}{Hg^0_{in}} = \frac{Hg^0_{in} - Hg^0_{out}}{Hg^0_{in}} \times 100\% \quad (1)$$

where Hg^0_{in} and Hg^0_{out} represent Hg^0 at the inlet and outlet of the reactor, respectively. All or part of the ΔHg^0 is captured on the catalysts as solid phase and the rest escapes to the gas phase. Thus, the Hg capture efficiency (E_{cap}) is always less than or equal to E_{oxi}, with E_{cap} calculated as

$$\begin{aligned} E_{cap}(\%) &= \frac{\Delta Hg^T}{Hg^T_{in}} \\ &= \frac{Hg^T_{in} - Hg^T_{out}}{Hg^T_{in}} \times 100\% \text{ or } E_{cap}(\%) \\ &= \frac{Hg^0_{in} - Hg^T_{out}}{Hg^0_{in}} \times 100\% \end{aligned} \quad (2)$$

where Hg^T_{in} and Hg^T_{out} represent Hg^T at the inlet and outlet of the reactor, respectively. Note that in this study $Hg^T_{in} = Hg^0_{in}$ and $Hg^T_{out} \geq Hg^0_{out}$.

Results and Discussion

Characterization of the Catalysts. The BET specific surface areas of the catalysts are listed in Table 2. All the catalysts

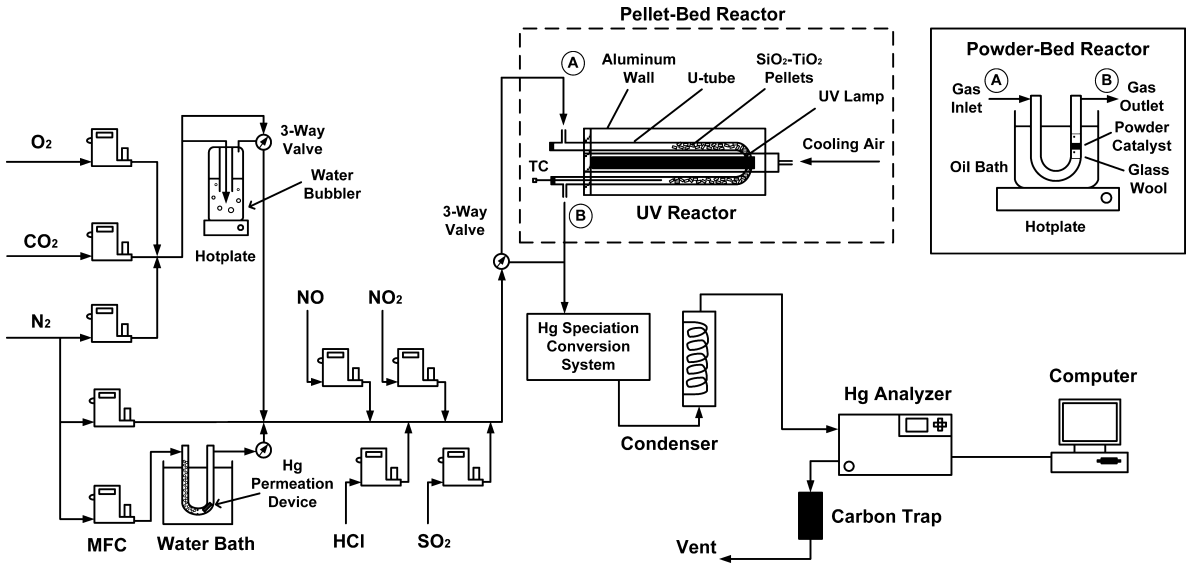

FIGURE 1. Experimental system for fixed-bed testing of catalysts.

TABLE 2. Catalysts Characterization and Their Activities on Hg Removal

sample	BET specific surface area (m^2/g)	surface V^{5+}/V (mol %)	surface V^{4+}/V (mol %)	V_2O_5/TiO_2 mass ratio	Hg oxi. rate[a] (μg/g-hr)	Hg cap. rate[a] (μg/g-hr)	E_{oxi}[b] (%)	E_{cap}[b] (%)
Silica gel	341.8							
ST12	319.4							
SV2	263.4				3.8	3.8	11	11
SV5	283.2	91.7	8.3		12.7	12.5	47	46
SV8	273.8	90.1	9.9		17.7	14.0	77	68
SV10	262.9	87.2	12.8		14.4	10.5	69	50
ST12V2	258.0			0.17	19.8	12.6	87	65
ST18V5	263.3			0.28	18.2	13.5	83	72
ST12V5	262.5	83.9	16.1	0.42	19.6	8.7	85	35
ST6V5	268.2			0.83	21.7	9.7	99	43

[a] From tests in set II where 0.50 g of powder catalysts were used. [b] Recorded at the end of the 6-h test in set II.

exhibit high surface areas (>250 m^2/g). Without any doping, the pure silica gel had the highest surface area. The inclusion of 12% TiO_2 to the silica gel (ST12) slightly reduced the surface area. The doping of V_2O_5 (2−10%) to the silica gel moderately reduced the surface area, but all the $SiO_2-V_2O_5$ catalysts had a similar level of surface areas. It is not clear why there is no apparent trend between the surface area and V_2O_5 loading. The surface areas of the $SiO_2-TiO_2-V_2O_5$ catalysts were close to those of the $SiO_2-V_2O_5$ catalysts.

The XRD patterns of the catalysts are shown in Figure 2. No discernible crystal phase of V_2O_5 (peak at $2\theta = 26.1°$) was detected for SV2 and SV5, which indicated that the vanadium contents were highly dispersed on these catalysts (*15*). A very small peak of crystalline V_2O_5 was detected for SV8, whereas SV10 showed a relatively broader and more prominent peak of crystalline V_2O_5. Molecular structures of vanadium oxides at different surface loadings have been reported in literature. As surface vanadia concentration increases, monomeric vanadyl species, polymeric vanadates, and aggregated amorphous/crystalline V_2O_5 clusters are subsequently formed (*12, 13, 23*). The XRD results in this study indicated that crystalline V_2O_5 becomes distinguishable as the vanadia loading increases to somewhere between 5 and 8%. The XRD pattern of ST12 showed a strong anatase phase (peaks at $2\theta = 25.3°$ and 38.0°) and a weak rutile phase (peak at $2\theta = 27.6°$) of TiO_2. Both ST12V5 and ST18V5 exhibited no crystal phase of V_2O_5, but ST18V5 had more prominent TiO_2 phases than ST12V5 because of the higher TiO_2 loading.

The oxidation states of vanadium species (V^{5+} and/or V^{4+}) in the catalysts were identified by XPS analysis as shown in Table 2. For SV5, SV8, and SV10, V^{5+} dominates (~90%) the vanadium content. Combining with the XRD results, it may imply that monomeric vandyl (V^{4+}) species transformed to polymeric vanadates (V^{5+}) as V_2O_5 loading increased to over 5%. For ST12V5, the fraction of V^{5+} was a little less than that in SV5. However, there could be errors involved in the quantitative analysis due to the overlap of binding energies (peaks) of V^{5+} and V^{4+} species as well as the interference from nearby O1s satellite peak (*23*).

Mercury Removal Using Pellet Catalysts. Tests were first performed and showed that pure silica pellets were inert to Hg removal and that homogeneous oxidation of Hg in the gas-phase was negligible under the experimental conditions. Figure 3 demonstrates Hg oxidation and capture efficiencies (E_{oxi} and E_{cap}) using different pellet catalysts (set I). For ST12 in FG1, there was negligible removal of Hg without UV light. With UV, E_{oxi} and E_{cap} were around 50%. In contrast, the activities of SV2 and ST12V2 on Hg removal were almost the same with or without UV irradiation. Thus, only the results without UV are shown for SV2 and ST12V2. Both SV2 and ST12V2 demonstrated very high efficiencies of Hg oxidation and capture (~90%), although their specific surface areas are lower than ST12 (Table 2). Apparently, the addition of V_2O_5 is advantageous due to the enhancement in chemisorption of Hg^0. It also simplifies the system by eliminating

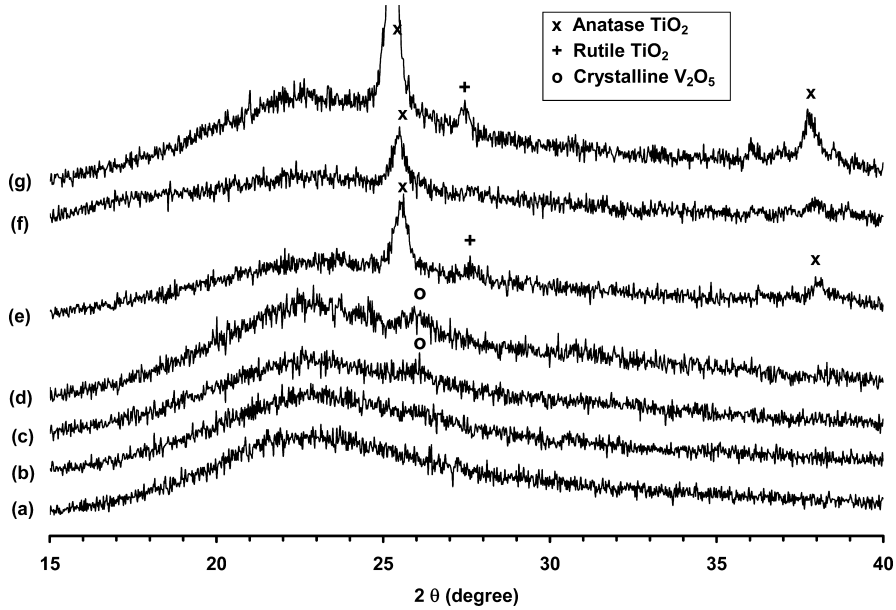

FIGURE 2. XRD patterns of (a) SV2, (b) SV5, (c) SV8, (d) SV10, (e) ST12, (f) ST12V5, and (g) ST18V5.

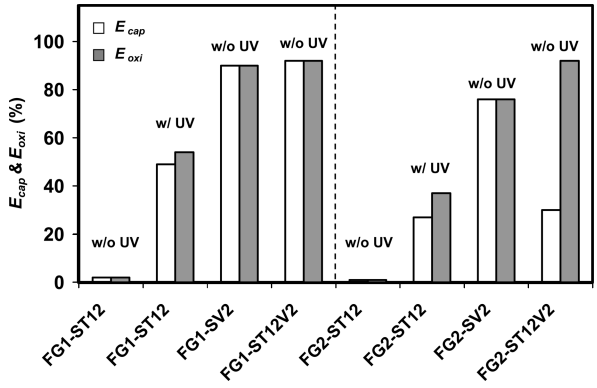

FIGURE 3. Hg Capture and oxidation efficiencies using pellet catalysts under simulated flue gas conditions FG1 and FG2.

the UV devices and reduces the cost by saving the energy of UV irradiation.

In FG2, the catalysts behaved in a similar pattern as in FG1, i.e., E_{oxi} of both SV2 and ST12V2 were much higher than ST12. Generally, E_{oxi} and E_{cap} in FG2 are less than in FG1, most likely due to the lower HCl and higher H_2O concentrations in FG2. It should be noted that for ST12V2, E_{cap} was much lower than E_{oxi} in FG2. This may be because that a larger fraction of certain volatile Hg compounds (such as mercuric nitrate, $Hg(NO_3)_2$) were produced.

Mercury Removal Using Powder Catalysts. No UV light was used for the study of powder catalysts since vanadia based catalysts do not need UV light activation. Tests were also performed to verify that the glass wools (used as the support of powders) and pure silica powders were inert to Hg removal. Then, experiments (set II) were carried out in FG3 using 500 mg of each catalyst (corresponding to a bed height of 17 mm) in a 6 h test. The profiles of normalized Hg concentration as a function of time for selected catalysts, SV8 and ST12V5, are shown in Figure 4. At the beginning Hg^T_{in} and Hg^0_{in} were measured and they were very close to each other. Then the flue gas passed through the reactor and Hg^T_{out} and Hg^0_{out} were measured. Hg^T_{in} and Hg^0_{in} were rechecked after a 6 h period. For SV8, Hg^T_{out} initially dropped to a very low level (E_{cap} = 93%), and then it increased and maintained relatively stabile at around 32% of Hg^T_{in} (E_{cap} = 68%). Hg^0_{out} was found to be slightly lower than Hg^T_{out}, indicating that a small portion of the oxidized Hg penetrated the reactor. E_{oxi}

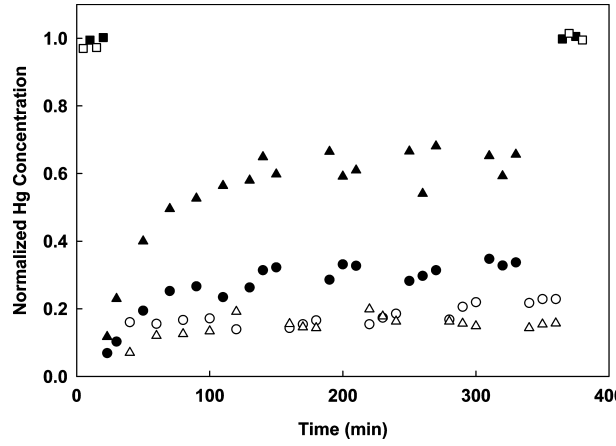

FIGURE 4. Hg concentration at the reactor outlet as a function of time using 500 mg powder catalysts (SV8 and ST12V5) under simulated flue gas condition FG3. Legend: ■, Hg^T_{in}; □, Hg^0_{in}; ●, Hg^T_{out}-SV8; ○, Hg^0_{out}-SV8; ▲, Hg^T_{out}-ST12V5; △, Hg^0_{out}-ST12V5.

was around 77% at the end of the 6 h test for SV8. Results for other $SiO_2-V_2O_5$ catalysts are summarized in Table 2. The Hg oxidation and capture rates averaged in the 6 h period increased as the V_2O_5 loading increased from 2 to 8% but decreased as the V_2O_5 loading further increased to 10%. E_{oxi} and E_{cap} measured at the end of the test followed the same trend. This suggested that the V_2O_5 loading for an optimal catalytic activity is somewhere near 8%. Combining the XRD and XPS results, it is inferred that the optimal V_2O_5 loading may be coincident with the maximum coverage of polymeric vanadates on the catalyst surface (5−8% V_2O_5). This is inline with the literature that the SCR activity of polymeric vanadates was much higher than that of monomeric vanadyl species, particularly at low temperatures (*12, 15*). While little literature has compared the activity of polymeric vanadates with crystalline V_2O_5, results in this study suggested that crystalline V_2O_5 is not superior to polymeric vanadates for Hg^0 oxidation.

For ST12V5 (Figure 4), Hg^0_{out} remained almost constantly low at 15% of Hg^0_{in} (E_{oxi} = 85%). Hg^T_{out} initially dropped to 11% of Hg^T_{in} but quickly increased and stabilized around 65% (E_{cap} = 35%). Comparing the four $SiO_2-TiO_2-V_2O_5$ catalysts (Table 2), the rates of Hg oxidation and capture are not an apparent function of the mass ratio of V_2O_5/TiO_2. All the $SiO_2-TiO_2-V_2O_5$ catalysts exhibited high oxidation efficiencies (E_{oxi}

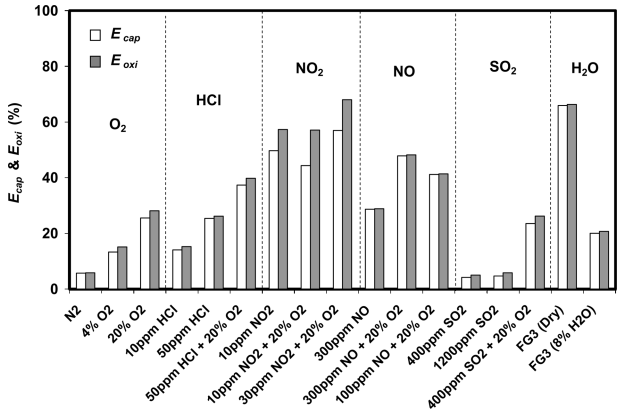

FIGURE 5. The role of flue gas components on Hg removal using 250 mg SV5 powder catalyst (all gases balanced with N_2).

> 83%) with ST6V5 having extremely high efficiency (E_{oxi} = 99%). It should be noted that the composition of FG3 is in the range of those flue gases burning low rank coals. Hence, the results implied that applications of the $SiO_2-TiO_2-V_2O_5$ catalysts can be beneficial to coal-fired power plants equipped with wet FGDs even burning low rank coals. The $SiO_2-TiO_2-V_2O_5$ catalysts generally exhibit greater abilities of oxidizing Hg compared to the $SiO_2-V_2O_5$ catalysts, although their Hg capture abilities (E_{cap}) are not always superior to the $SiO_2-V_2O_5$ catalysts with the same V_2O_5 loading. This enhanced oxidizing ability is in line with the literature where the SiO_2-TiO_2 supported V_2O_5 has a higher activity than SiO_2 supported V_2O_5 for reduction of NO (*24*). It is possible that the V−O−Ti bonds are more active than the V−O−Si bonds for Hg oxidation, since the V−O-support bonds are the most critical structures for catalytic oxidation in vanadia based catalysts (*13*).

Mercury Removal Mechanisms. To explore the Hg removal mechanisms on the $SiO_2-V_2O_5$ catalyst, experiments (set III) were conducted by mixing Hg with individual flue gas components and/or in combination with O_2, balanced with N_2. 250 mg of fresh SV5 was used in each test since it was found in set II that 5% V_2O_5 is close to the optimal loading. The results are summarized in Figure 5.

Role of O_2. Using high purity N_2 (>99.995%, Airgas) as the carrier gas without O_2, very little Hg removal was detected. This indicated that Hg is not physically adsorbed on the $SiO_2-V_2O_5$ catalyst in pure N_2. E_{oxi} increased to about 15% when 4% O_2 was introduced, and E_{oxi} further increased to 26% as O_2 increased to 20%. Granite et al. (*25*) studied various metal oxides for catalytic Hg removal and proposed that lattice oxygen of the metal oxides can serve as the oxidant of Hg, forming mercuric oxide (HgO). It has also been reported that lattice oxygen is the most abundant reactive intermediates that are responsible for oxidative dehydrogenation of alkanes over V_2O_5-based catalysts (*26*). Gas-phase O_2, on the other hand, reoxidizes the reduced metal oxides, replenishing the lattice oxygen (*25, 26*). The redox cycle can be summarized as follows:

$$V_2O_5 + Hg \rightarrow V_2O_4 + HgO \quad (3)$$

$$V_2O_4 + \frac{1}{2}O_2 \rightarrow V_2O_5 \quad (4)$$

The overall reaction then becomes

$$Hg + \frac{1}{2}O_2 \rightarrow HgO \quad (5)$$

Role of HCl. HCl was found to enhance Hg^0 oxidation over the $SiO_2-V_2O_5$ catalyst. Ten ppm HCl resulted in 15% Hg^0 oxidation, whereas 50 ppm HCl increased E_{oxi} to 25%. The combination of 50 ppm HCl with 20% O_2 further improved E_{oxi} to 39%. Parfitt et al. (*27*) found that HCl can adsorb on rutile surface generating hydroxyl (OH) groups on the surface which further react with excess HCl to form Cl ions and water. It has also been reported that Hg oxidation on unburned carbon or SCR catalysts occurs via an Eley−Rideal mechanism, where adsorbed HCl reacts with gas-phase (or weakly adsorbed) Hg^0 (*9, 28*). Following the Eley−Rideal mechanism, the reaction of HCl with the V_2O_5 surface occurs via

$$V-O-V + HCl \leftrightarrow V-OH-V-Cl \quad (6)$$

$$V-OH + HCl \leftrightarrow V-Cl + H_2O \quad (7)$$

Actually, the V−OH structures are one type of the active sites readily present on the surface of vanadia based catalysts (*12, 14, 29*). Thus, the reaction with HCl can directly start from Reaction 7. The chemically adsorbed Cl species then react with gas-phase Hg^0 to generate an intermediate HgCl species, which then further reacts with chlorine species to form a more stable mercuric chloride, $HgCl_2$. The overall reaction can be written as follows:

$$\frac{1}{2}O_2 + 2HCl + Hg \xrightarrow{V_2O_5} HgCl_2 + H_2O \quad (8)$$

It should be noted that chlorination of Hg may take place without the presence of O_2, as shown in Figure 5. In this case, V_2O_5 is consumed to form V_2O_4. The addition of 20% O_2 to 50 ppm HCl enhanced the total oxidation of Hg^0, very likely due to the oxidation of V_2O_4 to V_2O_5, i.e., the regeneration of the catalyst.

Role of NO_2. The effect of NO_2 was also found to be promotional. In the presence of 10 ppm NO_2, 57% of Hg was oxidized, whereas 50% was captured. When 20% O_2 was added, E_{oxi} remained at a similar level. Increasing NO_2 concentration to 30 ppm (with 20% O_2) increased E_{oxi} to 68% and E_{cap} to 57%. It has been reported that NO_2 significantly improves heterogeneous oxidation of Hg^0 on fly ash (*30*) and on activated carbon based sorbents (*31*). Other researchers have reported that adsorption of NO_2 on TiO_2 supported V_2O_5 catalysts was the first step in the process of selective catalytic reduction of NO_x (*12, 29*). Kantcheva et al. (*29*) indicated two pathways for the NO_2 adsorption on V_2O_5 involving *V*=O and V−OH sites:

$$V^{5+}=O + N^{4+}O_2 \rightarrow V^{4+}N^{5+}O_3 \quad (9)$$

$$2V^{5+}OH + 3NO_2 \rightarrow 2V^{5+}NO_3 + H_2O + NO \quad (10)$$

In this work, NO_2 is first adsorbed on V_2O_5 via Reactions 9 and 10 and then transformed to adsorbed nitrate species, which react with gaseous Hg^0 to form $Hg(NO_3)_2$ via the Eley−Rideal mechanism. The overall reaction can be written as follows:

$$O_2 + 2NO_2 + Hg \rightarrow Hg(NO_3)_2 \quad (11)$$

Considering the low melting point of $Hg(NO_3)_2$, 79 °C, it is likely that the product is volatile at the reactor temperature (135 °C) and thus part of it may be released from the reactor in the gas-phase. This formation of volatile $Hg(NO_3)_2$ initiated by NO_2 is in agreement with the findings by other researchers. Using a carbon-based sorbent to remove Hg^0, Miller et al. (*31*) observed nearly 100% breakthrough of a volatile oxidized Hg species in a gas mixture of SO_2 and NO_2. This volatile Hg species was identified to be $Hg(NO_3)_2$ in a follow-up study conducted by Olson et al. (*32*). Considering the much higher melting/decomposing point of $HgCl_2$ (277 °C) and HgO (500 °C), the penetration of these two less volatile Hg species is less likely.

Role of NO. As illustrated in Figure 5, E_{oxi} was 29% in the presence of 300 ppm NO, and an addition of 20% O_2 further

increased E_{oxi} to 48%. E_{oxi} and E_{cap} increased with the increase of NO concentration. Decreasing the NO concentration to 100 ppm moderately decreased the Hg^0 removal. It is generally agreed that NO adsorbs as nitrosyl and dinitrosyl surface species on reduced vanadia surfaces (*14*). The adsorbed NO can be oxidized on the surface, giving rise to species like NO^+, NO_2, and NO_3^-, or it can be reduced by reduced catalyst centers (*14*). It is likely that these adsorbed species derived from NO are responsible for the observed Hg^0 oxidation in this study, but the exact reaction pathways and products are unknown.

Role of SO_2. Figure 5 shows that the effect of SO_2 on Hg removal was insignificant at 400−1200 ppm. When combining 20% O_2 with 400 ppm SO_2, E_{oxi} and E_{cap} were very close to that without SO_2. In the literature, the effect of SO_2 on Hg capture in flue gas is not conclusive; either promotional or inhibitory effects over activated carbon or fly ash have been reported (*30, 33*). Hence, further studies combining SO_2 with other flue gas components would warrant a better understanding of the role of SO_2 for Hg removal on the $SiO_2-V_2O_5$ catalyst.

Role of H_2O. H_2O was found to inhibit Hg removal over $SiO_2-V_2O_5$ catalysts. As shown in Figure 5, under flue gas conditions (FG3) using 250 mg SV5, E_{oxi} decreased from 66 to 20% when the gas was switched from dry to humid (8% H_2O). Results of other two tests (not shown in Figure 5) indicated that the inhibitory effect of H_2O at very low concentration 0.6% is also observable. For a gas with 10 ppm HCl and 20% O_2, switching the gas from dry to 0.6% H_2O caused a decrease in E_{cap} from 30 to 19%. For another gas with 10 ppm NO_2 and 20% O_2, the introduction of 0.6% H_2O caused a decrease in E_{cap} from 43 to 24%. The competitive adsorption of water vapor on active sites may have prohibited the adsorption of reactive species such as HCl and NO_x, as reported in our previous studies (*19, 21*). It should be noted that this series of tests merely aimed to study the mechanisms; thus, only 0.25 g of SV5 was used. The inhibitory effect of H_2O can be mitigated when using more active catalysts with a larger amount, e.g., 0.5 g $SiO_2-TiO_2-V_2O_5$ catalysts, as demonstrated in set II experiments (Table 2). In addition, in a full flue gas, the promotional effects of HCl, NO, and NO_2 on Hg^0 oxidation, as previously demonstrated, may outweigh the adverse effect of H_2O.

Acknowledgments

We thank VICI Metronics, Inc. for supplying the Hg permeation device, and Sameer Matta, Jie Gao, and Qi Zhang for assisting with the experiments and chemical analysis.

Literature Cited

(1) U.S. EPA. *Mercury Study Report to Congress*, EPA-452/R-97−003; U.S. EPA: Washington, DC, 1997.
(2) U.S. EPA. Clean Air Mercury Rule, 40 CFR Parts 60, 63, 72, and 75; U.S. EPA: Washington, DC, 2005.
(3) http://www.epa.gov/mercury; Accessed March 19, 2008.
(4) Romero, C. E.; Li, Y.; Bilirgen, H.; Sarunac, N.; Levy, E. K. Modification of boiler operating conditions for mercury emissions reductions in coal-fired utility boilers. *Fuel* **2006**, *85*, 204–212.
(5) Jones, A. P.; Hoffmann, J. W.; Smith, D. N.; Feeley, T. J.; Murphy, J. T. DOE/NETL's phase II mercury control technology field testing program: Preliminary economic analysis of activated carbon injection. *Environ. Sci. Technol.* **2007**, *41*, 1365–1371.
(6) Presto, A. A.; Granite, E. J. Survey of catalysts for oxidation of mercury in flue gas. *Environ. Sci. Technol.* **2006**, *40*, 5601–5609.
(7) Senior, C. L. Oxidation of mercury across selective catalytic reduction catalysts in coal-fired power plants. *J. Air Waste Manage. Assoc.* **2006**, *56*, 23–31.
(8) Lee, C. W.; Srivastava, R. K.; Ghorishi, S. B.; Karwowski, J.; Hastings, T. W.; Hirschi, J. C. Pilot-scale study of the effect of selective catalytic reduction catalyst on mercury speciation in Illinois and powder river basin coal combustion flue gases. *J. Air Waste Manage. Assoc.* **2006**, *56*, 643–649.
(9) Niksa, S.; Fujiwara, N. A predictive mechanism for mercury oxidation on selective catalytic reduction catalysts under coal-derived flue gas. *J. Air Waste Manage. Assoc.* **2005**, *55*, 1866–1875.
(10) Richardson, C.; Machalek, T.; Miller, S.; Dene, C.; Chang, R. Effect of NOx control processes on mercury speciation in utility flue gas. *J. Air Waste Manage. Assoc.* **2002**, *52*, 941–947.
(11) Blythe, G.; Richardson, C.; Strohfus, M.; Lee, A.; Rhudy, R.; Lani, B. Pilot Testing of Oxidation Catalysts for Enhanced Mercury Control by Wet FGD. In *Proceedings of the U.S. Environmental Protection Agency-Department of Energy-EPRI Combined Power Plant Air Pollutant Control Symposium*; The MEGA Symposium: Washington DC, 2004.
(12) Parvulescu, V. I.; Grange, P.; Delmon, B. Catalytic removal of NO. *Catal. Today* **1998**, *46*, 233–316.
(13) Weckhuysen, B. M.; Keller, D. E. Chemistry, spectroscopy and the role of supported vanadium oxides in heterogeneous catalysis. *Catal. Today* **2003**, *78*, 25–46.
(14) Busca, G.; Lietti, L.; Ramis, G.; Berti, F. Chemical and mechanistic aspects of the selective catalytic reduction of NOx by ammonia over oxide catalysts: A review. *Appl. Catal., B* **1998**, *18*, 1–36.
(15) Kobayashi, M.; Kuma, R.; Morita, A. Low temperature selective catalytic reduction of NO by NH_3 over V_2O_5 supported on TiO_2-SiO_2-MoO_3. *Catal. Lett.* **2006**, *112*, 37–44.
(16) Kobayashi, M.; Kuma, R.; Masaki, S.; Sugishima, N. TiO_2-SiO_2 and V_2O_5/TiO_2-SiO_2 catalyst: Physico-chemical characteristics and catalytic behavior in selective catalytic reduction of NO by NH_3. *Appl. Catal., B* **2005**, *60*, 173–179.
(17) Pitoniak, E.; Wu, C. Y.; Londeree, D.; Mazyck, D.; Bonzongo, J. C.; Powers, K.; Sigmund, W. Nanostructured silica-gel doped with TiO_2 for mercury vapor control. *J. Nanopart. Res.* **2003**, *5*, 281–292.
(18) Wu, C. Y.; Lee, T. G.; Tyree, G.; Arar, E.; Biswas, P. Capture of mercury in combustion systems by in-situ generated titania particles with UV irradiation. *Environ. Eng. Sci.* **1998**, *15*, 137–148.
(19) Li, Y.; Murphy, P.; Wu, C. Y. Removal of elemental mercury from simulated coal-combustion flue gas using a SiO_2-TiO_2 nanocomposite *Fuel Process. Technol.* **2008**, *89*, 567–573.
(20) Li, Y.; Wu, C. Y. Kinetic study for photocatalytic oxidation of elemental mercury on a SiO_2-TiO_2 nanocomposite. *Environ. Eng. Sci.* **2007**, *24*, 3–12.
(21) Li, Y.; Wu, C. Y. Role of moisture in adsorption, photocatalytic oxidation, and reemission of elemental mercury on a SiO_2-TiO_2 nanocomposite. *Environ. Sci. Technol.* **2006**, *40*, 6444–6448.
(22) Pitoniak, E.; Wu, C. Y.; Mazyck, D. W.; Powers, K. W.; Sigmund, W. Adsorption enhancement mechanisms of silica-titania nanocomposites for elemental mercury vapor removal. *Environ. Sci. Technol.* **2005**, *39*, 1269–1274.
(23) Rodella, C. B.; Nascente, P. A. P.; Franco, R. W. A.; Magon, C. J.; Mastelaro, V. R.; Florentino, A. O. Surface characterisation of V_2O_5/TiO_2 catalytic system. *Phy. Status Solidi A* **2001**, *187*, 161–169.
(24) Shikada, T.; Fujimoto, K.; Kunugi, T.; Tominaga, H.; Kaneko, S.; Kubo, Y. Reduction of nitric-oxide with ammonia on vanadium-oxide catalysts supported on homogeneously precipitated silica-titania. *Ind. Eng. Chem. Prod. Res. Dev* **1981**, *20*, 91–95.
(25) Granite, E. J.; Pennline, H. W.; Hargis, R. A. Novel sorbents for mercury removal from flue gas. *Ind. Eng. Chem. Res.* **2000**, *39*, 1020–1029.
(26) Grabowski, R.; Pietrzyk, S.; Sloczynski, J.; Genser, F.; Wcislo, K.; Grzybowska-Swierkosz, B. Kinetics of the propane oxidative dehydrogenation on vanadia/titania catalysts from steady-state and transient experiments. *Appl. Catal., A* **2002**, *232*, 277–288.
(27) Parfitt, G. D.; Ramsboth, J.; Rocheste, C. H. Infra-red study of hydrogen chloride adsorption on rutile surfaces. *Trans. Faraday Soc.* **1971**, *67*, 3100–3109.
(28) Niksa, S.; Fujiwara, N. Predicting extents of mercury oxidation in coal-derived flue gases. *J. Air Waste Manage. Assoc.* **2005**, *55*, 930–939.
(29) Kantcheva, M.; Bushev, V.; Klissurski, D. Study of the NO_2-NH_3 interaction on a titania (anatase) supported vanadia catalyst. *J. Catal.* **1994**, *145*, 96–106.
(30) Norton, G. A.; Yang, H. Q.; Brown, R. C.; Laudal, D. L.; Dunham, G. E.; Erjavec, J. Heterogeneous oxidation of mercury in simulated post combustion conditions. *Fuel* **2003**, *82*, 107–116.
(31) Miller, S. J.; Dunham, G. E.; Olson, E. S.; Brown, T. D. Flue gas effects on a carbon-based mercury sorbent. *Fuel Process. Technol.* **2000**, *65*, 343–363.
(32) Olson, E. S.; Sharma, R. K.; Pavlish, J. H. On the analysis of mercuric nitrate in flue gas by GC-MS. *Anal. Bioanal. Chem.* **2002**, *374*, 1045–1049.
(33) Laudal, D. L.; Brown, T. D.; Nott, B. R. Effects of flue gas constituents on mercury speciation. *Fuel Process. Technol.* **2000**, *65*, 157–165.

ES8000272